Spray velocity field analysis with Optical Flow Method – An alternative to Particle Image Velocimetry

S. Lorenz*[1], J. Goldlücke[2], D. Straub[1], D. Brüggemann[1]
1. Lehrstuhl für Technische Thermodynamik und Transportprozesse, Universität Bayreuth, Germany
2. Goldlücke Ingenieurleistungen, Germany
sebastian.lorenz@uni-bayreuth.de, juergen.goldluecke@giib.de, lttt@uni-bayreuth.de, and brueggemann@uni-bayreuth.de

Abstract

There are various optical measurement methods to determine the flow field of sprays. In this work the Optical Flow Method (OFM) is applied to high speed recordings of a gasoline direct injection fuel spray. Since sophisticated results can be achieved even by simple assembling, OFM demonstrates a promising alternative to commonly used methods. For example quantities of transient and turbulent flows can be obtained by only using a high speed camera in connection with an intense white light source. Due to the possibility to analyze an entire injection process measurements can be restricted to one exposure per cycle. The used technique for OFM is founded on a method by Horn and Schnuck and is compared to the approved method of Particle Image Velocimetry (PIV). Therefore two experimental setups are realized in which the OFM is applied to recordings of a light sheet as well as shadowgraphy recordings. The simultaneously taken PIV at fixed times during injection shows comparable results to OFM. Presenting various examples, assets and drawbacks as well as the principal differences of each method are shown. It turns out that the OFM has a great potential for spray analysis at higher densities and at increased chamber temperature levels.

Introduction

During the last few years, analysis of atomization and sprays has become more and more important as indicated by the increasing number of publications dealing with this topic. Two main reasons can be identified for this development. On the one hand an increasing number of alternative fuels have entered the market. These fuels show a different spray pattern if they are used with existing gasoline or diesel injectors and engines [1,2]. Consequently it is important to measure the different spray parameters resulting from changed surface tension and viscosity quickly and as easily as possible. On the other hand, significant work has been done to reduce fuel consumption, NO_x emissions and PM (particulate matter) by improving the use of conventional fuels [3,4]. Main approaches are further development of injection strategies, like boot or pilot injection [5,6], or higher injection pressures [7]. The principle purpose is to improve the mixing process of fuel and air and to controlling the spray to wall contact [8].

There are numerous optical methods for spray characterizing which are often roughly divided into classical measurement techniques like visualization [9,10], Particle Image Velocimetry (PIV) [11], Laser Induced Fluorescence [12] and Phase Doppler Anemometry [13], and "emerging" techniques like Light Sheet Dropsizing [14], Molecular Tagging Velocimetry [15], Ballistic Imaging [16] and X-ray Imaging[17]. A comparison of the classical measurement techniques is given by S. N. Soid and Z. A. Zainal [18], which shows that these techniques are often hard to implement, very expensive or, in case of pure visualization, limited to measurements of macroscopic parameters like spray angle or penetration depth. Furthermore, A. Coghe et al. [19] and E. Berrocal [20] compare classical measuring technologies with emerging methods regarding their applicability to measure sprays with high density and reveal that most of the classical methods are poorly suited for an application in optical dense sprays or in regions with high spray density. Using the emerging methods, high experimental efforts are often necessary or the techniques, like X-ray radiography, are too expensive for many laboratories.

This paper introduces a new method for a simple determination of the spray velocity field based on the analysis of the optical flow. The combination of spray illumination and a high speed camera enables this technique for determining the spray velocity field during the whole injection process with only one single measurement. This is advantageous to determine cycle-to-cycle variations of the fuel spray. Due to the principle of the Optical Flow Method (OFM) to analyze moving spray structures, the presence of single particles or droplets in the spray is not necessary and additionally the method contains a high potential for analyzing dense sprays.

* Corresponding author: lttt@uni-bayreuth.de

To evaluate OFM in this paper, the method is compared to the established PIV [21]. The measurements are carried out in an optically accessible spray chamber and the flow field of a gasoline injector for direct injection serves as a measurement object. Furthermore, it is shown how new methods for spray analyzing can quantitatively and qualitatively be validated.

In the first section of this paper each method is explained. Subsequently two setups for simultaneously measuring with OFM and PIV are presented. Various examples in the following result section point out the assets and drawbacks as well as the principal differences of each method. Thus an objective evaluation of the OFM can be provided in the conclusion of this paper.

Numerical Methods

Two methods are presented in this work to determine the flow field of a spray. On the one hand the high speed recording of the spray is analysed by the Optical Flow Method, on the other hand the recognized and reliable method of Particle Image Velocimetry is used as a reference.

The determination of flow fields using PIV is based on the ability of liquid droplets to follow the movement of the fluid [11]. Therefore the spray is illuminated two times with an 8 ns laser light sheet. The laser intensities and the temporal laser pulse spacing depend on the density, the maximum velocity as well as the velocity gradients. After acquiring the image data of the spray, the image pair is divided into image segments which are subsequently evaluated by a cross correlation function in connection with Fast Fourier Transformation in order to speed up calculation time. As a result, the function provides a displacement vector for each image segment. The velocity can be calculated from the time difference between the two images. The smallest size of the evaluated image segments depends on the number of particles in the image and on the value of the velocity gradient. Hence a defined number of vectors can be determined for the overall image. An overlap of the image segments was selected which increases the vector density. The applied PIV software Davis 7.0 works with complementary methods in order to reduce incorrectly determined vectors in the calculated flow field. Within this work, multipass iterations with decreasing grid size are used. At the first mesh size a 50% overlap and a dual assessment is chosen. Subsequently, the calculation was performed towards a smaller mesh size applying a 25% overlap and a triple assessment. In addition, every unit of the grid is weighted by a circular Gaussian function. Thus the center of each square exerts the majority of the influence. The cross correlation was conducted using a Fast Fourier Transformation (FFT) additionally taking the Wiener-Khintchine theorem into account. In order to avoid falsification of the results, complementary methods like smoothing, vector supplements or vector plausibility checks are not applied.

The methodology of optical flow analysis utilizes the apparent motion of brightness patterns in an image sequence to deduce a vector field [22]. If brightness patterns (intensity difference) are present in the image sequence and only change moderately from image to image, the movement of each pixel can be assessed. The regularly cited optical flow methods can be roughly assigned by three basic methods: The so-called “matching methods” work similar to the above mentioned PIV analysis by splitting the frames into a large number of windows followed by application of either cross correlation or the least squares method. The vector field had to be smoothed or filters had to be applied before or after the optical flow analysis. Filter based methods rely on the assumption that a recorded motion influences the frequency spectrum generated by the Fourier transformation. The third differential method uses intensity gradients in the grey tone distribution and is the method of choice presented in this work. The motion of all pixels in the image is calculated in reference to each other. An important advantage consists in the direct implementation of smoothing or other pre- and post processings within a global term. Thus an independent calculation is no longer required. The movement of the points can be calculated with the boundary condition that intensities of moving points do not change from image to image:

$$I(x, y, t) = I(x + \partial x, y + \partial y, t + \partial t) \tag{1}$$

In this equation, *x* and *y* denote the position within the image and *t* refers to time dimension. From a Taylor expansion of (1) the well-known brightness constancy constraint equation (BCCE) can be derived:

$$\frac{\partial I}{\partial x} v_x + \frac{\partial I}{\partial y} v_y + \frac{\partial I}{\partial t} = \nabla I \cdot \vec{v} + \frac{\partial I}{\partial t} = 0 \tag{2}$$

This under-determined equation is not sufficient to evaluate the unknown velocity vectors v_x and v_y. Local approaches to solve this problem are based on the assumption that the optical flow is constant in a small area and can be obtained a solution by minimizing the energy functional:

$$E(\vec{v}) = \iint_{\Omega} \left(\frac{\partial I}{\partial x} v_x + \frac{\partial I}{\partial y} v_y + \frac{\partial I}{\partial t} \right)^2 dxdy \tag{3}$$

Horn und Schunck present another solution to the problem [23]. They combined equation (2) with a global smoothness term and integrated over the whole image:

$$E(\vec{v}) = \iint_{\Omega} \left(\frac{\partial I}{\partial x} v_x + \frac{\partial I}{\partial y} v_y + \frac{\partial I}{\partial t}\right)^2 + \left(\|\nabla v_x\|_2^2 + \|\nabla v_y\|_2^2\right) dxdy \quad (4)$$

This technique is called "global" because energy cannot be optimized locally. But due to the isotropic influence of the smoothness, edges and strong grey tone gradients are smoothed as well. Preserving important image information, different approaches work with an anisotropic smoothness term [24]. In this work a weighting function set up by Charbonnier et al. [25] was used:

$$g(\|\nabla I\|_2^2) = \left(1 + \frac{\|\nabla I\|_2^2}{e_s^2}\right)^{-0,5} \quad (5)$$

The small positive and arbitrary contrast parameter e_s allows controlling the strength of the anisotropy. Thereby the gradient of the grey tone intensity dynamically modifies the amount of smoothness and the image structure is preserved. The resulting energy functional reads:

$$E(\vec{v}) = \iint_{\Omega} \left(\nabla I \cdot \vec{v} + \frac{\partial I}{\partial t}\right)^2 + \lambda^2 \, g(\|\nabla I\|_2^2)\left(\|\nabla v_x\|_2^2 + \|\nabla v_y\|_2^2\right) dxdy \quad (6)$$

The influence of the smoothness term can now be varied by an isotropic parameter λ and by the anisotropic weighting function. Motion vectors can be derived from minimization of the energy functional. Euler-Lagrange-Equations provide the solution of this minimization problem. Subsequently a system of coupled non-linear differential equations is obtained, which has to be solved numerically. Unidirectional multigrid methods are promising as they rely on advantageous settings of the initial grid values. Computational load of the minimization problem is significantly reduced by predefined sub-sampling factors. After each calculation level the result is implemented into the next higher level. Due to this technique a refined approximation is obtained level by level. This strategy enables the evaluation of large image sequences with low computing time. The calculation results in a vector field of velocities for each image sample in the sequence. By choosing data and smoothing term in this manner and with image sequences comprising more than two individual images, post-processing of the results becomes dispensable since owing to the optimization problem the best-possible solution over the image sequence is calculated. The results presented in this work are calculated with the image processing Software PIX!CEL from a sequence of three images. The number of iterations can be enhanced up to 10 steps. But usually no noticeable deviations can be observed after one to three steps. Taking high-speed images at high frame rates leads to low image resolution. In order to receive significant results even at high frame rates doubling the picture resolution of OFM is an approved approach.

Experimental Methods

The experiments are performed in an optically accessible spray chamber capable of operating at pressures up to 10 bar and at temperatures up to 500 K (figure 1). The high pressure gasoline injector (Bosch, HDEV 1) is coupled with a high pressure pump which applies a constant fuel pressure of 100 bar to the injector. The heatable bottom plate is exchangeable to adjust different angles for spray-wall interactions.

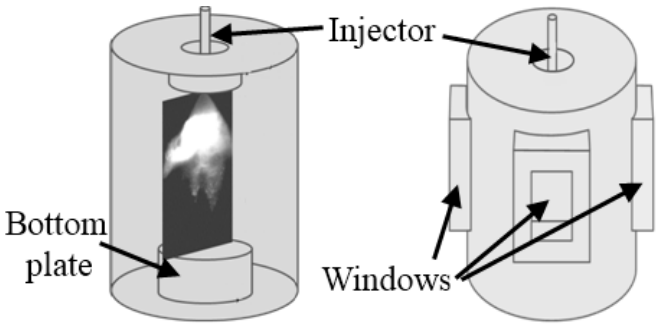

Figure 1. Schematic of the optically accessible spray chamber for various pressures with gasoline injector and heatable bottom plate.

In a first step OFM and PIV are compared by two simultaneously taken light sheet recordings of the gasoline spray formation (figure 2). This was realized by a superposition of the light from a continuous Ar^+-laser (514 nm) for OFM high speed recordings and a frequency doubled Nd:YAG double pulse laser (532 nm) for PIV. Therefore the two laser beams were overlapped by a dichroic mirror, widened to a thin light sheet and positioned in the center of the spray. The Mie scattering is selected by appropriate optical filters to the high-speed camera and to a two frame PIV camera. The high-speed recordings were taken with a CMOS camera (Photron, Fastcam APX 120K) with a resolution depending on the frame rate. It varies from 256 × 256 pixels in the case of 15.000 fps to 256 × 64 pixels in the case of 50.000 fps. The camera resolution of the PIV camera (LaVision, Flowmaster 3S) is constant at 1280 × 1024 pixels. The time delay between the two frames was selected between 5 to 15 µs depending on the droplet motion.

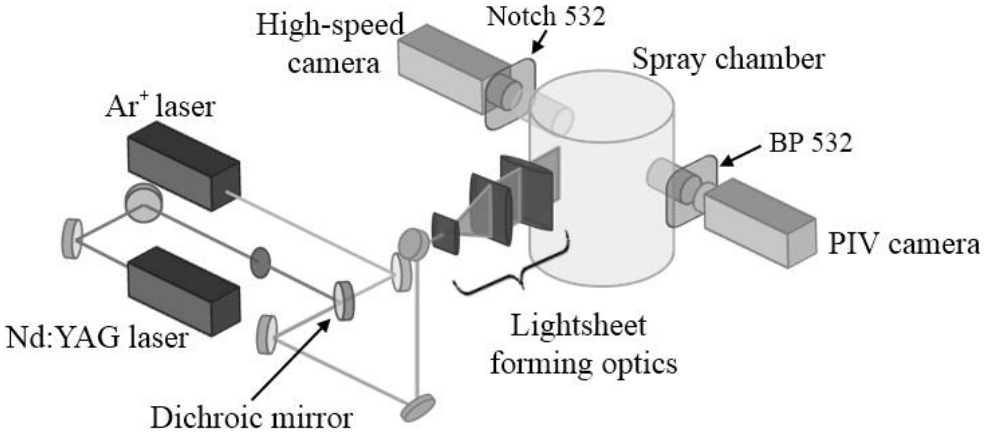

Figure 2. Schematic of the first optical setup with two laser sheets.

In the second part of this work it is shown that for spray analysis using optical flow method neither Mie scattering nor a laser is necessary at all. The only requirement is a sufficient illumination of the spray. In order to illustrate this, a second experimental setup was developed (figure 3).

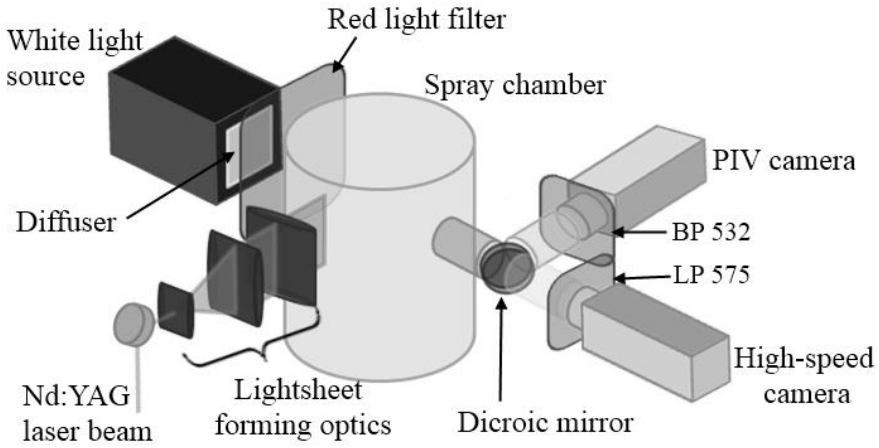

Figure 3. Schematic of the second optical setup with a laser sheet and back illumination.

Using a white light source, the spray was continuously back illuminated. A LED-array-radiator with diffuser serves as such a light source and provides uniform illumination. The arising shadow was recorded by a high-speed camera. The well-established method PIV was used similarly to the first setup in order to verify the results. A red light filter was placed in front of the white light source to separate the continuous light from the pulsed green MIE-scattering light. The light of the PIV laser was diverted to the PIV camera by a dichroic mirror that is placed on the other side of the spray chamber. The undesirable radiation is suppressed additionally by means of optical filters arranged in front of the cameras.

Both experimental setups use a central trigger unit for controlling the two cameras, the double pulse laser and the injector. Consequently a precise chronological assignment of all recorded images and sequences of images was possible. In order to avoid undesirable spray ignition by the laser, the chamber was rinsed with nitrogen before each measurement.

Results and Discussion

The results published in this paper have been selected in such a way that capabilities as well as assets and drawbacks of OFM can be demonstrated. Furthermore, the principle differences between OFM and PIV are set in contrast to each other in a comparative way. Firstly the two methods are compared by using two light sheets on the gasoline spray and detecting the Mie scattering as described above in setup one. Therefore two PIV images were taken at a defined time after the visible start of injection (VSOI). Via high speed camera an image sequence is taken simultaneously and the three suitable images are chosen for OFM. Figure 4 shows the resulting velocity fields of the spray 1000 µs after VSOI. The time intervals for calculating these fields differ from principles. Due to the negligible exposure time of 8 ns the time interval for PIV equals the image time distance of 4 µs. The OFM uses three images at frame rate of 15.000 fps and an exposure time of 66 µs, which leads to an observation period of 200 µs. Because of the motion blur a detection of single droplets is not possible in this case. In contrast to PIV the motion blur presents no problem for OFM. The scale of the velocity fields can be applied to all following results in this paper. The comparison of figure 4 a) and figure 4 b) shows that the vector directions of the fields correlate well. However, there are minor differences between OFM and PIV at the strong intensity edge on the lower left side of the spray (figure 4 b). These differences result from the aperture problem of OFM. By using more than three images for OFM and an increased time interval, this effect could be minimized but the comparability to PIV is increasingly lost in this experiment. Due to the analysis of grey tone motion, OFM yields detailed results at the outside edge of the spray. If, however, small droplets are pushed out of the spray cone, the velocity gradient in these areas rapidly increases. This can cause analyzing problems with PIV which have to be corrected by pre- and post-processing to achieve more detailed results in the vector field. The relatively large vector grid size of 32 × 32 pixels in figure 4 a) prevents the display of such obviously incorrect vectors. There are also differences between the presented methods of analyzing the sac spray. Due to the dilute character of the spray in this area with only a few droplets, PIV shows advantages of analyzing the droplet motion here. By the use of continuous Mie scattering in combination with quite long exposure times, these single droplets cannot be detected by the high-speed camera and are consequently not available for OFM. Thus figure 4 b) shows only a weak reflection of this structure.

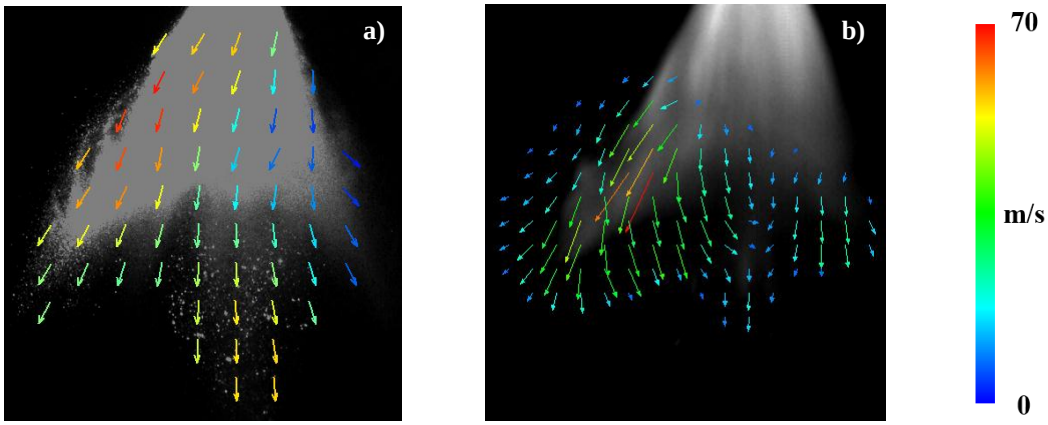

Figure 4. Velocity field 1000 µs after VSOI at normal conditions, (a) light sheet analyzed by PIV, (b) light sheet analyzed by OFM. Velocity illustrated with colors, in case of OFM additionally with arrow length.

In the next step, the vector quantities of figure 4 a) and figure 4 b) are compared. At the lower edge areas, the values show good agreement with each other (green colored vectors). The few fast droplets in the center below the spray cone can only be analyzed by PIV. Therefore the resulting vector quantities are incomparable to the ones determined in figure 4 b). In the left wing of the spray comparable maximum velocity values can be calculated with each method (orange and red colored vectors). Due to the temporal constant brightness pattern in the taken high-speed image sequence the upper part of the spray is not suitable for OFM. A solution consists in optimizing the illumination for these regions or changing the type of spray illumination. The first suggestion can be realized by increasing the laser power which leads to an increasing background radiation in the simultaneously taken images for PIV. Changing the type of illumination is realized in the second setup, see next paragraph. In conclusion the flow analysis by particle motion with PIV has advantages compared to OFM in these regions up to a specific spray density. Yet, the available PIV system has the disadvantage of receiving only a single velocity field per injection process. The development of so-called high-speed PIV systems [26–30] can solve this problem but requires more sophisticated and expensive equipment. An analysis of the complete injection process is successful without any additional effort by the use of OFM.

In the second part of this work, the OFM is applied to high speed shadowgraphy of the gasoline spray. For this optical technique a laser may be employed, but is no longer required. The sufficiency of a strong diffuse white light source has an important advantage for industrial applications where laser based systems are avoided due to significant safety measures. In the results presented below the rotationally symmetrical spray cone is examined. Additionally, a spray-wall interaction is realized using a 17° inclined bottom plate. Figure 5 shows the two resulting velocity fields 1600 µs after VSOI at normal conditions of 1 bar absolute ambient pressure and 298 K ambient temperature. At that time the injector closes and the spray breaks up from the nozzle. The wall contact takes place shortly before this time. The vector field calculated by PIV well illustrates the flow in the upper regions of the spray (figure 5 a). There are no problems with intensity gradients caused by the spray breakup from the nozzle. However, the vectors near the bottom plate show no consistent direction. The most probable explanation of this effect is the interaction of droplets bouncing back with droplets coming directly from the nozzle. Pre- and post-processing can be used to minimize or hide the undesirable vectors.

The vector field analyzed by OFM is shown in figure 5 b). Due to large intensity gradients caused by the spray breakup, the vectors near the nozzle are slightly overvalued. A higher frame rate and concentration of this region would or more frames for calculation prevent this effect. In the middle region of the spray as well as near the bottom plate, the global propagation can easily be recognized because of the global analyzing character of the OFM. Apart from the discussed obviously false vectors, the vectors analyzed by the two methods are similar in absolute value and direction.

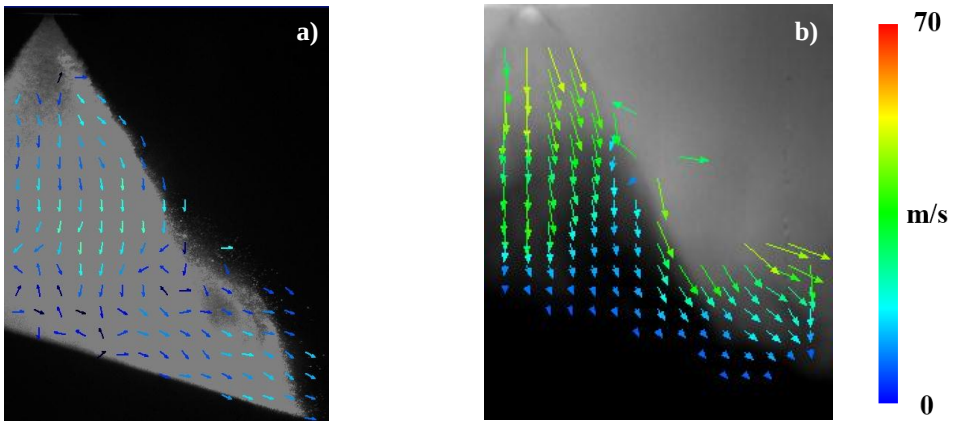

Figure 5. Velocity field 1600 µs after VSOI at normal conditions, (a) light sheet analyzed by PIV, (b) shadowgraphy analyzed by OFM. Velocity illustrated with colors, in case of OFM additionally with arrow length.

In order to increase the spray density, the ambient pressure was raised to 5 bar absolute pressure. Figure 6 shows the resulting vector fields of a considerable compact spray. The beginning of the exposure time is set to 1600 µs after VSOI and is kept equal to figure 5. At the PIV vector field, stream lines were implemented for clarification. It can be seen that the spray spreads straight from the nozzle to the bottom. The spray angle is smaller than the one observed in figure 5. After the wall contact a spray eddy is built which moves along the sloping bottom plate. Due to the increased ambient pressure the droplets have a lower velocity and the droplet bouncing effect on the wall is smaller. Thus the vector directions near the bottom plate in figure 6 a) can be displayed correctly. In figure 6 b), showing OFM at the same time, the spray is optically dense. In order to assure the comparability to figure 5 and in order to show the direct effect of increasing optical spray density, the light intensity has deliberately not been increased. With the increasing light intensity the inner spray structures can easily be resolved like in figures 5 b) or 7 b). This shows that OFM can handle the optical dense spray and delivers detailed results in the area of the spray edge and the occurring wall eddy. The velocity vectors again show similar results to the PIV vectors with respect to absolute values and direction.

For further comparison, the ambient temperature was increased to 423 K instead of enhancing the ambient pressure. The time studied was 700 µs after VSOI. Figure 7 shows the resulting vector fields. Due to high temperatures, the spray evaporates quickly. With regard to PIV the separation of scattering particles and luminous spray fog consequently becomes very difficult. Therefore, obviously falsely interpreted vectors may result especially in dense spray regions, as can be seen in figure 7 a). However, this circumstance does not cause any problems for OFM. In this case it does not matter if moving intensity distribution is caused by droplets or a spray fog. Consequently, this method of analysis delivers a satisfactory vector field without any obvious errors.

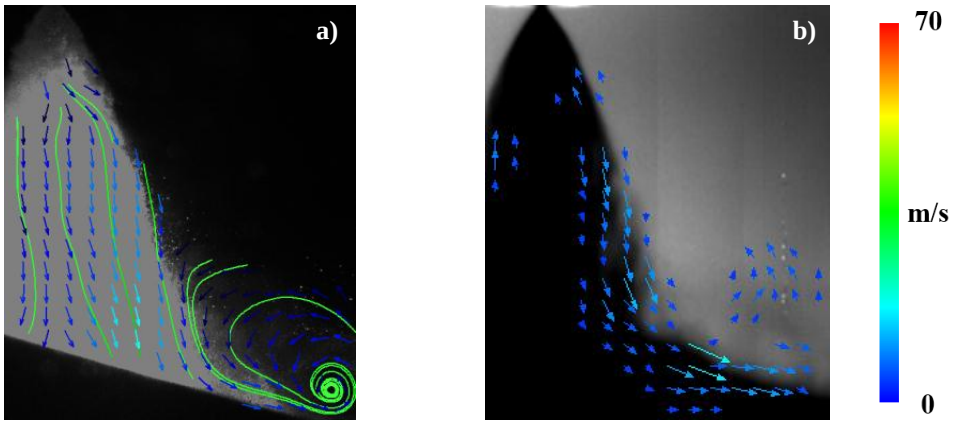

Figure 6. Velocity field 1600 µs after VSOI at 5 bar ambient pressure, (a) light sheet analyzed by PIV, (b) shadowgraphy analyzed by OFM. Velocity illustrated with colors, in case of OFM additionally with arrow length.

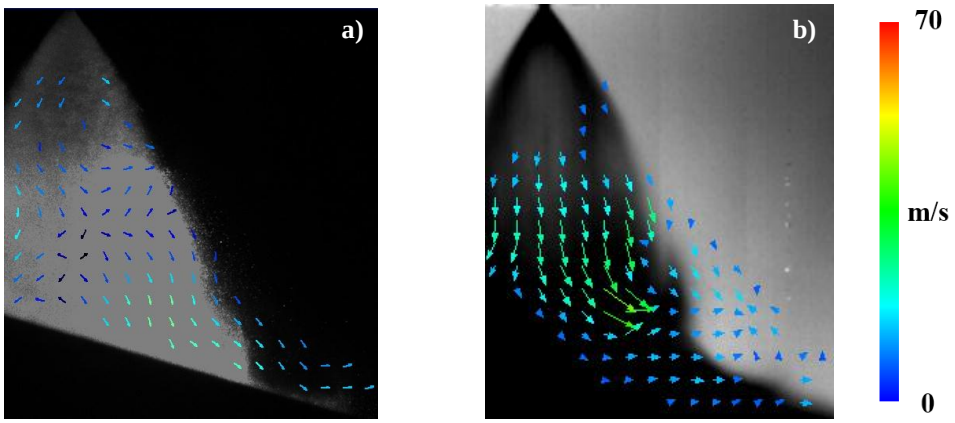

Figure 7. Velocity field 700 µs after VSOI at 423 K ambient temperature, (a) light sheet analyzed by PIV, (b) shadowgraphy analyzed by OFM. Velocity illustrated with colors, in case of OFM additionally with arrow length.

Finally, the capability of precisely analysing turbulence structures with OFM is presented. For this, moving wall eddies are illuminated by a thin sheet of light, which is induced by a continuous laser in the first setup (figure 2). In order to receive sufficient structure intensity for high-speed camera frame rate of 50.000 fps the laser power was increased to 1 W. Figure 8 a) shows the forming eddy shortly after spray impact onto the wall. Even if the translation motion mainly overshadows rotation, first signs of the eddy can clearly be seen. Due to surrounding air, droplets in the upper field of the eddy are slowed down and lose their translational motion. After 480 µs further spray translation (similar positions are denoted by the red line in figure 8 b)) the eddy is dominated by rotation. Such an analysis can be realized by the above mentioned OFM within only a single measurement. The image sequence taken here allows the calculation of 24 additional vector fields between figure 8 a) and b), which leads to an overall time resolution of 20 µs.

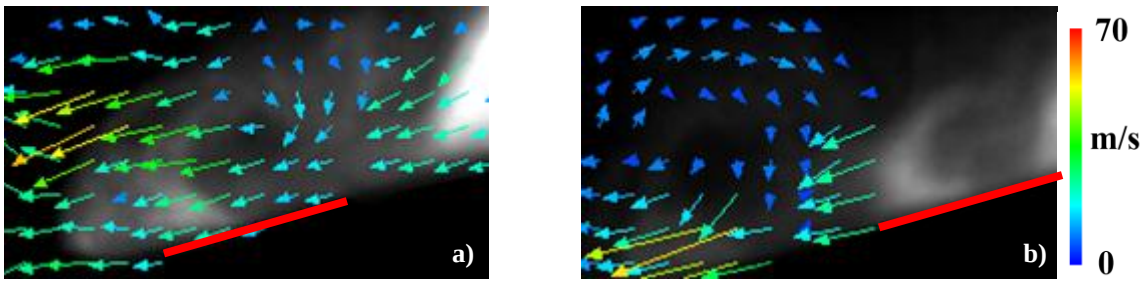

Figure 8. OFM of vertebral structures on a wall: (a) shortly after spray wall contact, (b) 480 µs after a). Velocity illustrated with colors, in case of OFM additionally with arrow length.

Summary and Conclusions

The Optical Flow Method (OFM) – a simple technique for analyzing spray velocity fields – was demonstrated and experimentally compared to simultaneously taken PIV measurements. Comparing two light sheets, the resulting vector fields of both methods correlate well despite small principal differences in the measuring time interval. Due to the high-speed recording, OFM can determine the spray velocity fields during the entire injection process with only one measurement in contrast to the applied PIV. High-speed PIV systems [31] are able to perform as well but are more expensive and require a higher experimental effort. In a second step the OFM was applied to high speed shadowgraphy and the spray observation was extended to spray-wall contact. It can be shown that a clear vector calculation by PIV is not possible if droplet motion near the wall varies too much in direction. Due to the global consideration of the spray in combination with longer measurement time, OFM shows a much better reproduction of velocity fields of the global spray expansion. Because of the strong intensity gradient with spray breakup at the nozzle, error corrections are necessary in OFM. The increase of ambient pressure leads to a more compact spray pattern. At the edges of this spray, the OFM field compares well with the field calculated by PIV. By intentionally choosing a low light illumination, it can be shown that for OFM a certain threshold of spray penetrating light is necessary to obtain the moving brightness patterns for analysis. Furthermore, a high bit-rate of the camera and an effective use of the grey tone scale provide better results. Increasing the ambient temperature, an optically transparent spray with a higher optical depth [20] can be generated. OFM shows advantages over PIV in spray areas where single droplets are indistinguishable. As a result, OFM has a great potential for analyzing optical transparent sprays with higher optical densities. In this context, further investigations of optical dense spray regions, e.g. in the zone near the nozzle, should clear the maximum optical depth for good OFM results. Since this method can be applied in connection with Schlieren Measurement Technique, flow analysis of a spray will be extended to vapor phase in the near future.

Acknowledgements

This work was supported in part by the Bayerische Forschungsstiftung (BFS).

References

[1] Gao J, Jiang D, Huang Z., *Fuel* 86:1645–50 (2007).
[2] Kannan GR, Anand R., *J. Renewable Sustainable Energy* 4:12703 (2012).
[3] Fang T, Coverdill RE, Lee CF, White RA., *Fuel* 87:3232–9 (2008).
[4] Wang X, Wang Z, Ni P, Wei S, Mao G., *Energy Procedia* 13:5697–702 (2011).
[5] Fang Q, Fang J, Zhuang J, Huang Z., *Applied Thermal Engineering* (2012).
[6] Luckhchoura V, Peters N, Diwakar R., *International Journal of Engine Research* 12:145–68 (2011).
[7] Wang X, Huang Z, Zhang W, Kuti OA, Nishida K., *Applied Energy* 88:1620–8 (2011).
[8] Andreassi L, Ubertini S, Allocca L., *International Journal of Multiphase Flow* 33:742–65 (2007).
[9] Chirgier N., *Progress in Energy and Combustion Science* 17:211–62 (1991).
[10] Shao J, Yan Y, Greeves G, Smith S., *Meas. Sci. Technol* 14:1110–6 (2003).
[11] Adrian RJ., *Exp Fluids* 39:159–69 (2005).
[12] Zhao H, Ladommatos N., *Progress in Energy and Combustion Science* 24:297–336 (1998).
[13] Albrecht H., *Laser doppler and phase doppler measurement techniques*, Berlin: Springer, 2003.
[14] Le Gal P, Farrugia N, Greenhalgh D., *Optics & Laser Technology* 31:75–83 (1999).
[15] Koochesfahani MM, Goh AC, Schock HJ., *The Aerodynamics of Heavy Vehicles: Trucks, Buses, and Trains* 19:143–55 (2004).
[16] Linne M, Sedarsky D, Meyer T, Gord J, Carter C., *Exp Fluids* 49:911–23 (2010).
[17] Linne M., *Exp Fluids* (2011).
[18] Soid S, Zainal Z., *Energy* 36:724–41 (2011).
[19] Coghe A, Cossali G., *Optics and Lasers in Engineering* 50:46–56 (2012).
[20] Berrocal E. *PhD Thesis*, Cranfield, 2006.
[21] Driscoll KD, Sick V, Gray C., *Experiments in Fluids* 35:112–5 (2003).
[22] Tchernykh V., *4th IFAC-Symposium on Mechatronic Systems.* Heidelberg, Sept. 12 - Sept. 14, 2006.
[23] Horn BK, Schunck BG., *Artifical Intelligence* 17:185–203 (1981).
[24] Nagel HH., *International Joint Conference on Artificial Intelligence*, 1983.
[25] Charbonnier P, Blanc-Feraud L, Aubert G, Barlaud M., *IEEE Trans. on Image Process* 6:298–311 (1997).
[26] Fajardo C, Sick V., *Exp Fluids* 46:43–53 (2009).
[27] Falchi M, Romano GP., *Exp Fluids* 47:509–26 (2009).
[28] Müller SHR, Böhm B, Gleißner M, Grzeszik R, Arndt S, Dreizler A., *Exp Fluids* 48:281–90 (2010).
[29] Upatnieks A, Laberteaux K, Ceccio SL., *Exp Fluids* 32:87–98 (2002).
[30] Williams TC, Hargrave GK, Halliwell NA., *Experiments in Fluids* 35:85–91 (2003).
[31] Sick V, Drake MC, Fansler TD., *Exp Fluids* 49:937–47 (2010).